RESEARCH ARTICLE

ADVANCED MATERIALS INTERFACES Open Access

www.advmatinterfaces.de

Enhancing Diamond Biosensors and Photonic Devices: The Interplay of Surface Roughness, Functionalization, and Fluorescence

Seyed Mohammad Mahdi Dadfar, Sylwia Sekula-Neuner, and Michael Hirtz**

Diamond holds exceptional promise in biosensing and quantum applications due to its unique physical, chemical, and electronic properties. This work addresses two critical aspects of diamond material utilization: surface functionalization for biosensors and surface roughness effects on fluorescence. First, this study introduces a novel biosensor approach, preparing oxygen-terminated diamond surfaces with controlled roughness (4 and 14 nm) and functionalizing them via esterification and silanization to generate DBCO-, thiol-, and epoxy-terminated surfaces. These are used to immobilize microarrays of fluorescent and non-fluorescent inks through click chemistry. Optimal click reaction strategies are identified for streptavidin detection, demonstrating a stable and sensitive biointerface. Second, the influence of surface roughness are investigated on fluorescence intensity, revealing that smoother surfaces (4 nm) exhibit significantly enhanced fluorescence compared to rougher surfaces (14 nm). This enhancement is attributed to reduced light scattering and defect density. This integrated approach advances diamond-based technologies by optimizing surface properties for both biosensing and photonic applications.

1. Introduction

Diamond's superb mechanical, chemical, and electronic properties make it an exceptional material for diverse applications, including biosensing, quantum computing, photonics, and bioimaging. In particular, diamond biosensors are uniquely important due to their outstanding biocompatibility, chemical stability, and wide electrochemical potential window, which enable highly sensitive and reliable detection in complex biological environments, advantages not offered by conventional materials like silicon or gold. Key applications include neurotransmitter monitoring, DNA and protein detection, and neural interfacing, where diamond's stability and low background current are essential. While prior work has demonstrated diamond's promise in biosensing, challenges remain in achieving robust surface functionalization and scalable device fabrication, which this study aims to address.[1] Its remarkable hardness, wide electrochemical potential window, high optical transparency (UV to IR), and highest known thermal conductivity among semiconductors, coupled with its wide bandgap (≈5.5 eV), superior biocompatibility, and exceptional chemical stability, make it an ideal candidate for robust and long-lasting devices.[1a,2] The key challenge in diamond-based biosensor design is achieving stable and efficient surface functionalization to enable biomolecular interactions. For practical biophysical or diagnostic applications, it is crucial that the functionalization layer exhibits strong chemical stability and remains intact throughout the duration of a typical experiment.[3] Diamond is renowned for its ability to resist harsh chemical environments. Therefore, modifying diamond surfaces is more challenging compared to other semiconductor surfaces due to their chemical inertness to most agents, making the process significantly more difficult. Over the past several years, significant progress has been made in developing simple and highly specific surface modification methods for introducing various functional groups onto diamond surfaces.[4] Various methods are employed for surface functionalization, including silanization,[5] plasma treatment,[6] polymer grafting,[7] layer-by-layer (LbL) assembly,[8] sol-gel coating[9] and bioconjugation.[10] Among these, click chemistry offers a highly efficient and selective method for surface modification. This relatively recent advancement, introduced by Barry Sharpless and his colleagues in 2001, provides an efficient method for coupling organic and bioorganic molecules.

S. M. M. Dadfar, M. Hirtz
Institute of Nanotechnology (INT) and Karlsruhe Nano Micro Facility (KNMF)
Karlsruhe Institute of Technology (KIT)
Kaiserstraße 12, 76131 Karlsruhe, Germany
E-mail: Mahdi.Dadfar@esm.tu-freiberg.de; michael.hirtz@kit.edu

S. M. M. Dadfar
Institute of Nanoscale and Biobased Materials
Faculty of Materials Science and Technology
TU Bergakademie Freiberg
Gustav-Zeuner-Str. 3, 09599 Freiberg, Germany

S. Sekula-Neuner
n.able GmbH, Hermann-von-Helmholtz-Platz 1
76344 Eggenstein-Leopoldshafen, Germany

The ORCID identification number(s) for the author(s) of this article can be found under https://doi.org/10.1002/admi.202500378

DOI: 10.1002/admi.202500378

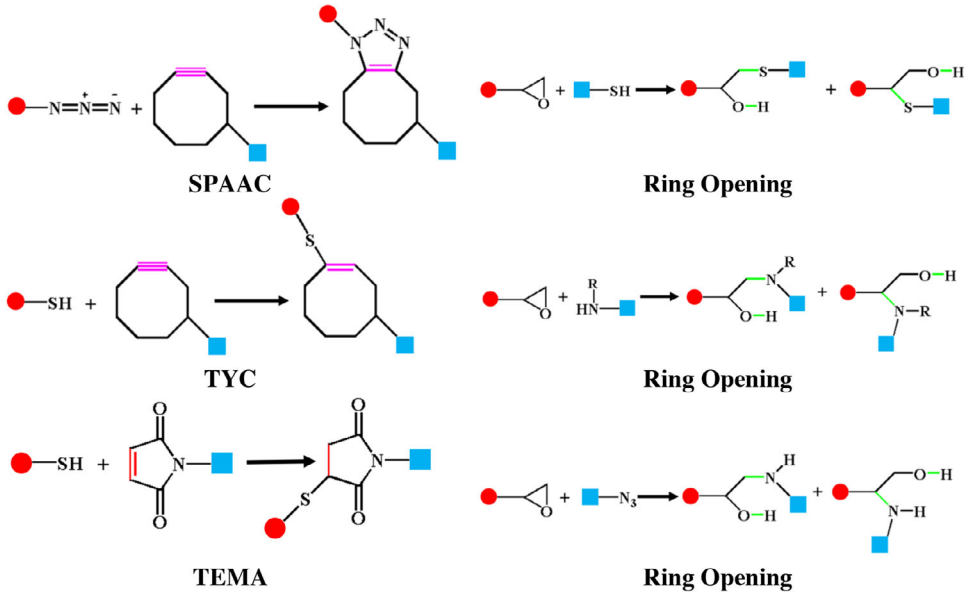

Figure 1. Selected types of click chemistry reactions: strain-promoted azide-alkyne cycloaddition (SPAAC), thiol-yne coupling (TYC), thiol-ene Michael addition (TEMA), and epoxy ring opening with thiols, amines, and azides, respectively.

In recognition of its significant impact, the Nobel Prize in chemistry was awarded in 2022 to Barry Sharpless and collaborators for their contributions to the development of click chemistry and bioorthogonal chemistry. Click chemistry involves the assembly of small molecular units through robust heteroatom linkages to create useful compounds. This reaction occurs rapidly, with high selectivity and efficiency, under mild conditions. It is typically carried out at room temperature and produces either no byproducts or only harmless ones. Furthermore, its compatibility with a wide range of solvents, particularly water, enhances its versatility and broad applicability.[11] Recent studies have demonstrated the utility of click chemistry in biosensor applications. Siegel et al. (2024) employed strain-promoted azide-alkyne cycloaddition (SPAAC) to functionalize nanoparticles with DNA,[12] while Wang et al. (2023) utilized thiol-ene click reactions to modify membranes for antifouling applications.[13] In 2022, Kumar et al. reported the use of clickable antifouling polymer coatings on diamond surfaces.[14] Furthermore, Mouzhe Xie and colleagues (2021) developed a robust, biocompatible silanization and SPAAC click chemistry strategy for biotin–streptavidin conjugation directly on single-crystal diamond sensors.[15] In another study, Martin-Gómez et al. (2021) leveraged copper(I)-catalyzed azide-alkyne cycloaddition (CuAAC) to functionalize various surfaces, including polylactic acid, gold, and titanium.[16] Additionally, Zhang et al. (2020) demonstrated a spontaneous, catalyst-free amino-yne click reaction for the efficient immobilization of proteins and cells on functionalized surfaces.[17] In our previous studies, we employed various types of click chemistry reactions for protein immobilization and the functionalization of glass surfaces. These click reactions, shown in **Figure 1**, include SPAAC, a reaction between azides and alkynes; thiol-ene Michael addition (TEMA), involving thiols and maleimides; thiol-yne coupling (TYC), a reaction between thiol and alkyne; and ring-opening reactions, which occur between azides, thiols, or amines with the epoxy group. For each click reaction, we explored various parameters that could influence its efficiency, such as temperature, reaction time, catalyst type, and catalyst concentration. The optimal reaction conditions for each click reaction were determined and are summarized in **Table 1**.[18] Building upon this foundation, the current study addresses two critical aspects: 1) We explore the integration of click chemistry with diamond-based biosensors, employing lithography-assisted functionalization to determine the most effective click reaction for protein binding. The step-by-step process for conducting experiments on different diamond

Table 1. Optimal reaction conditions for the probed types of click reactions as reported in the literature.

Fluorescent Ink	Glass Surface	Optimal Reaction Condition	Refs.
Cy5-thiol	DBCO-terminated	40 Min, 37 °C	[18a]
TAMRA-azide	DBCO-terminated	20 Min, 37 °C	[18a]
TAMRA-Mmaleimide	Thiol-terminated	20 Min, 37 °C, 10 mol% TEA to dye	[18c]
FAM-DBCO	Thiol-terminated	20 Min, 37 °C	[18c]
Cy5-thiol	Epoxy-terminated	40 Min, 37 °C, 10 mol% TEA to dye	[18b]
R6G	Epoxy-terminated	40 Min, 37 °C, 3 mol% $Bi(OTf)_3$ to dye	[18b]
TAMRA-azide	Epoxy-terminated	10 Min, 37 °C, 3 mol% $Bi(OTf)_3$ and 3 mol% Ph_3P to dye	[18b]

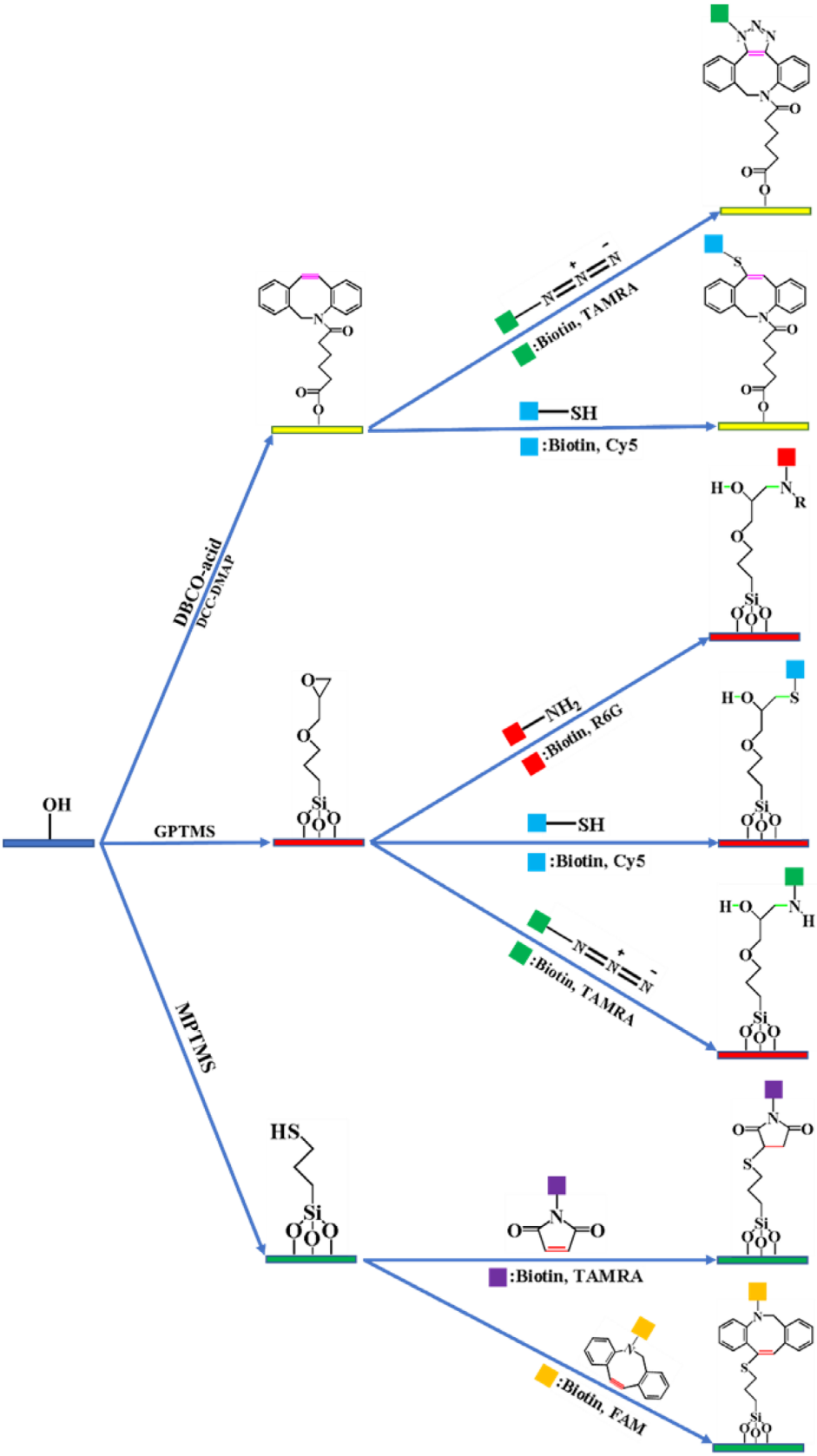

Figure 2. Schematic illustration of click reactions on DBCO-, epoxy-, and thiol-terminated diamond surfaces regarded in this work.

Table 2. List of chemicals used in this work.

Commercial name	Short name	Role	Source
Dibenzocyclooctyne-acid	DBCO-acid	Coupling agent in esterification	Jena Bioscience (Germany)
(3-Glycidyloxypropyl)trimethoxysilan	GPTMS	Coupling agent in silanization	Sigma–Aldrich (Germany)
(3-Mercaptopropyl)trimethoxysilan	MPTMS	Coupling agent in silanization	Sigma–Aldrich (Germany)
5-Carboxytetramethylrhodamine-azide	TAMRA-azide	Fluorescent dye	Jena Bioscience (Germany)
Dibenzylcyclooctyne-PEG_4-5/6-FAM	FAM-DBCO	Fluorescent dye	Jena Bioscience (Germany)
Cy5-labeled polyethylene glycol thiol	Cy5-thiol	Fluorescent dye	Nanocs Company (USA)
Tetramethylrhodamine-5-maleimide	TAMRA-maleimide	Fluorescent dye	Sigma–Aldrich (Germany)
Rhodamine 6G	R6G	Fluorescent dye	Sigma–Aldrich (Germany)
Streptavidin-Cy3	Streptavidin	Conjugation with biotinylated molecules	Sigma–Aldrich (Germany)
Azide-PEG_3-biotin conjugate	Biotin-azide	Nonfluorescent dye (biotinylated molecule)	Jena Bioscience (Germany)
Dibenzylcyclooctyne-PEG_4-Biotin	Biotin-DBCO	Nonfluorescent dye (biotinylated molecule)	Jena Bioscience (Germany)
Biotin polyethylene thiol	Biotin-thiol	Nonfluorescent dye (biotinylated molecule)	Nanocs Company (USA)
Biotin-dPEG®11-MAL	Biotin maleimide	Nonfluorescent dye (biotinylated molecule)	Sigma–Aldrich (Germany)
Biotin-dPEG®$_7$-NH_2	Biotin-amine	Nonfluorescent dye (biotinylated molecule)	Sigma–Aldrich (Germany)
4-dimethylaminopyridine	DMAP	Catalyst	Sigma–Aldrich (Germany)
Triethylamine	TEA	Catalyst	Sigma–Aldrich (Germany)
Bismuth(III) trifluoromethanesulfonate	$Bi(OTf)_3$	Catalyst	Sigma–Aldrich (Germany)
N,N′-dicyclohexylcarbodiimide	DCC	Catalyst	Sigma–Aldrich (Germany)
Bovine serum albumin	BSA	Blocker	Sigma–Aldrich (Germany)
Phosphate buffer saline	PBS	Buffer	Sigma–Aldrich (Germany)
Dimethyl sulfoxide	DMSO	Solvent	Sigma–Aldrich (Germany)
Glycerol	-	-	Sigma–Aldrich (Germany)

surfaces is illustrated in **Figure 2**. 2) In parallel, we investigate how nanoscale roughness variations influence fluorescence intensity. The interplay between surface roughness and fluorescence efficiency is crucial for optimizing diamond's performance in photonic and quantum applications. By systematically exploring surface modifications, immobilization strategies, and roughness effects, we aim to offer vital information for future advancements in diamond-based technologies.

2. Experimental Section

2.1. Materials

Table 2 lists the most important materials used in this study. All materials were used as received without further purification steps.

2.2. Preparation of Hydrogen- and Oxygen-Terminated Diamonds

Hydrogen- and oxygen-terminated diamonds were produced through a combination of hydrogen and oxygen plasma treatment and the chemical vapor deposition (CVD) method. Diamond growth begins with the deposition of a nanoparticle seed layer onto the substrate. This was achieved through ultrasonication for 30 min in a water-based suspension containing 0.1 wt.% ultra-dispersed nanodiamond particles, typically ranging from 5 to 10 nm in size. In the following, the samples were rinsed with deionized water and methanol. After being dried with a nitrogen stream, the wafer was transferred to an ellipsoidal microwave plasma reactor. The diamond films were grown using a gas mixture of 1% CH_4 in 99% H_2, at a pressure of 55 mbar, a microwave power of 3.5 kW, and a temperature of 850 °C. The growth rate was 1–2 µm h^{-1}. Following growth, the samples were cleaned in a concentrated HNO_3:H_2SO_4 solution to remove surface contaminants.[19]

2.3. Diamond Functionalization

Oxygen-terminated diamonds (1 cm × 1 cm) were rinsed with chloroform, 2-propanol, and deionized water, and dried under a nitrogen stream. Subsequently, to activate the diamond surfaces, they were exposed to oxygen plasma (10 sccm O_2, 0.2 mbar, and 100 W, ATTO system, Diener electronics, Germany) for 2 min. To generate epoxy and thiol-terminated diamonds, the obtained hydroxyl-terminated diamonds were immersed in a 2% (v/v) solution of GPTMS in dry toluene and a 2% (v/v) solution of MPTMS in dry toluene respectively for 5 h, at room temperature and after this time, the functionalized diamonds were removed from the solution, thoroughly rinsed with acetone, toluene, and deionized water, and dried under a stream of nitrogen. To produce DBCO-terminated diamonds, the hydroxyl-terminated diamonds were immersed in a DMSO solution containing DBCO-acid (0.02 mmol, 6.67 mg), DCC (0.022 mmol, 4.53 mg), and DMAP (0.0035 mmol, 0.43 mg) at room temperature for 24 h under a nitrogen atmosphere. The DBCO-terminated samples underwent sonication with DMSO (5 min, two times), ethanol (5 min, two times), and finally deionized water (5 min, two times). Then the samples were dried under a nitrogen stream.

2.4. Atomic Force Microscopy (AFM)

Mapping of roughness via AFM was performed on a Dimension Icon system (Bruker, Germany) in tapping mode with HQ:NSC15/Al BS cantilevers (MikroMasch, USA). The surface roughness values were determined using Atomic Force Microscopy (AFM) (NanoScope 8.10, Bruker, Germany) in air under ambient conditions. As a measure of roughness, the root-mean-square (RMS) average of height deviations from the mean image data plane (denoted as Rq in the software) was extracted from 5 × 5 μm^2 scan areas. For each data point, measurements were taken from four different regions, and the average RMS roughness was calculated. The reported roughness values of 4 and 14 nm were achieved by applying two distinct mechanical polishing protocols prior to surface cleaning and functionalization: the smoother surface (4 nm) was obtained through fine mechanical polishing, whereas the rougher surface (14 nm) resulted from a coarser polishing process.

2.5. Contact Angle Measurements

Static contact angles were measured at room temperature using an OCA-20 contact angle analyzer (Data Physics Instruments GmbH, Germany). For each measurement, five water droplets with the same volume and rate (2 µL and 2 µL s^{-1}, respectively) were dropped on the surface and the average value of the contact angle was reported.

2.6. Ink Solution Preparation

The fluorescent and non-fluorescent dyes (Biotin compounds) used for the µCS were TAMRA-azide (λ_{abs} = 546 nm, λ_{em} = 579 nm) and biotin-azide for doing SPAAC click reaction, Cy5-thiol (λ_{abs} = 650 nm, λ_{em} = 670 nm) and biotin-thiol for doing TYC on DBCO-terminated diamond. FAM-DBCO (λ_{abs} = 492 nm, λ_{em} = 517 nm) and biotin-DBCO for doing TYC, TAMRA-maleimide (λ_{abs} = 543 nm, λ_{em} = 575 nm) and biotin-maleimide for doing TEMA on the thiol-terminated diamond. Cy5-thiol, R6G (λ_{abs} = 530 nm, λ_{em} = 556 nm), TAMRA-azide, biotin-thiol, biotin-amine, and biotin-azide for doing ring opening on epoxy-terminated diamond. All dyes were dissolved in a DMSO/glycerol mixture (7:3) at concentrations of 500 µg mL^{-1} for fluorescent dyes and 1000 µg mL^{-1} for non-fluorescent dyes.

2.7. Pattern Writing via µCS

The spotting procedures were conducted using the NLP 2000 system (NanoInk, USA) equipped with SPT pens (SPT-S-C10S, Bioforce Nanosciences). Before use, the pen was freshly plasma cleaned by oxygen plasma (10 sccm O_2, 0.2 mbar, 100 W, 2 min) and used immediately. The pen reservoir was filled with 0.2 µL of the ink solution. The spotting procedures were carried out at a relative humidity of 20%. For all patterns, a dwell time of 2 s was used.

2.8. Protein Binding on Microarrays

The binding of fluorescently-labeled streptavidin to arrays of different types of biotin-conjugates immobilized on differently functionalized diamonds via click reaction was examined. Before adding the streptavidin solution, the samples were blocked with 10% bovine serum albumin (BSA) in PBS for 30 min to avoid unspecific streptavidin binding around the microarrays. Following that, the samples were washed three times by pipetting on and off 30 µL of PBS and then incubated for 1 h with a solution of 10 µg mL^{-1} of streptavidin in a dark environment. Afterward, the samples were washed three times by pipetting on and off PBS, rinsed with deionized water, and were then dried with nitrogen blowing before examination using fluorescence microscopy.

2.9. Fluorescence Microscopy Technique

The fluorescence imaging was conducted using a Nikon Eclipse 80i upright fluorescence microscope (Nikon, Japan) equipped with an Intensilight illumination (Nikon, Japan), a CoolSNAP HQ2 camera (Photometrics, USA), and a set of filters named FITC (λ_{abs} = 475 nm, λ_{em} = 530 nm, color-coded green), Texas Red (λ_{abs} = 559 nm, λ_{em} = 630 nm, color-coded red), and Cy5 λ_{abs} = 604 nm, λ_{em} = 712 nm, color-coded purple). Subsequently, using the onboard software (NIS-Elements, Nikon, Japan) the average fluorescence intensity per feature was measured, and the obtained results were tabulated for the preparation of diagrams and statistical analysis.

2.10. Statistical Analysis

All data were expressed as the means plus standard deviations. The significant differences between treatments were analyzed using one-way ANOVA and Duncan tests ($p < 0.05$) with the statistical package for the social sciences (SPSS, version 19.0.0 Abacus Concepts, Berkeley, California, USA).

3. Result and Discussion

3.1. Surface Roughness and Morphology

Atomic force microscopy (AFM) was employed to measure the surface roughness of a set of diamond samples prepared to obtain a low (polished) and high (as synthesized) roughness surface for comparison. The measured surface roughness values for the two diamond samples were 4 and 14 nm, respectively (**Figure 3**), indicating distinct surface topographies also on visual inspection of the AFM topography images. Sample 1, with a significantly lower roughness of 4 nm, exhibits a much smoother surface. In contrast, Sample 2, with a higher roughness value of 14 nm, features a relatively uneven surface characterized by pronounced peaks and valleys. These differences in surface characteristics show the effectiveness of the post-treatment processes, such as polishing or etching, which can significantly influence surface morphology.[20]

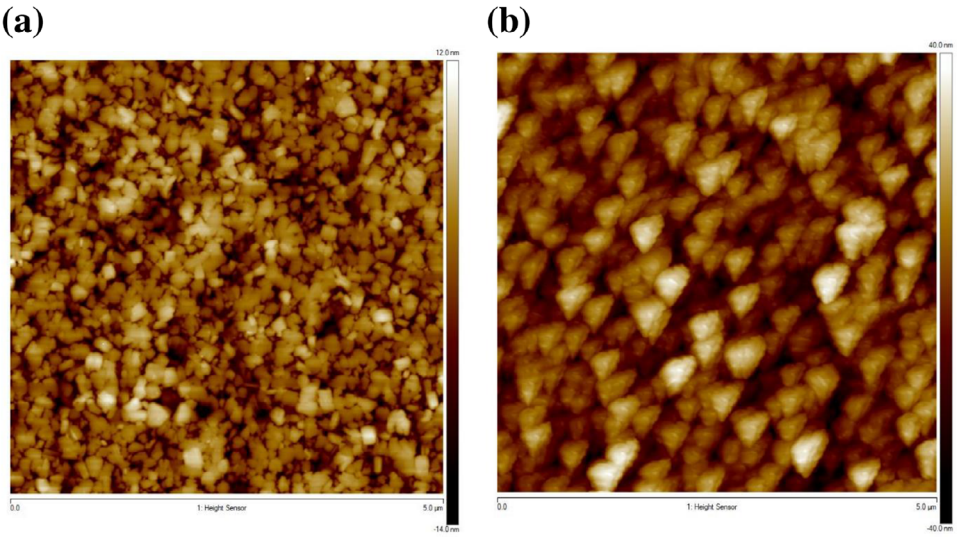

Figure 3. AFM images of two diamond surfaces with an average roughness (RMS) of a) 4 nm and b) 14 nm.

3.2. Surface Wetting on Functionalized Diamond Surfaces

To achieve successful spotting and high-resolution arrays on functionalized diamond surfaces, the contact angle of water droplets on the surface should not be too low, as otherwise the spotted inks will spread and no ordered arrays can form. The contact angles for hydrogen-, oxygen-, DBCO-, thiol-, and epoxy-terminated diamond surfaces are presented in Figure 4. The contact angle of water on the surfaces remained stable over time (measured after 24 days), showing no significant changes. Interestingly, a notable difference was observed between the two roughness levels for both hydrogen- and oxygen-terminated surfaces. The increase in contact angle with increasing surface roughness, from 4 to 14 nm, can be attributed to the amplification of intrinsic surface wettability due to nanoscale topography, as explained by the Wenzel and Cassie-Baxter models. Increased roughness enhances the intrinsic wetting characteristics of the surface, and at the nanometer scale, it can also lead to partial air entrapment beneath the droplet, especially on hydrophilic (oxygen-terminated) surfaces, resulting in higher apparent contact angles. This phenomenon has been reported in studies on diamond surfaces, where both hydrophobic and hydrophilic terminations exhibit increased contact angles with higher roughness due to a combination of increased surface area, possible air pocket formation, and surface heterogeneity.[21] Additionally, the oxygen-terminated surface exhibited a lower contact angle than the hydrogen-terminated one, suggesting that oxygen plasma treatment introduces a layer of hydroxyl groups, increasing hydrophilicity. However, after functionalization with MPTMS, GPTMS, or DBCO, the contact angle increased. The increase in angle after functionalization could be attributed to several factors. The introduced chemicals modify the surface chemistry of the diamond, replacing the original termination (e.g., hydrogen or oxygen) with new functional groups like

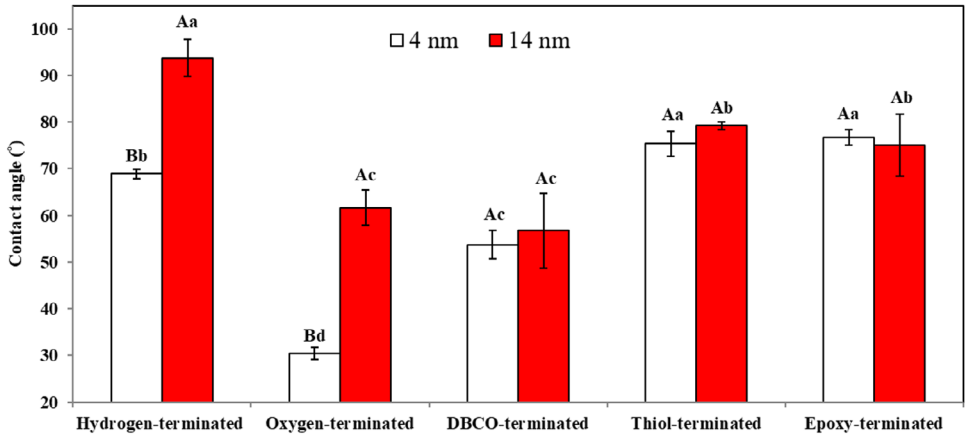

Figure 4. Contact angle measurement for the different types of functionalized diamond surfaces. For the same roughnesses, contact angle bars with different lower case letters and for the same functional groups, values with different capital letters are significantly different (p <0.05), according to Duncan's test.

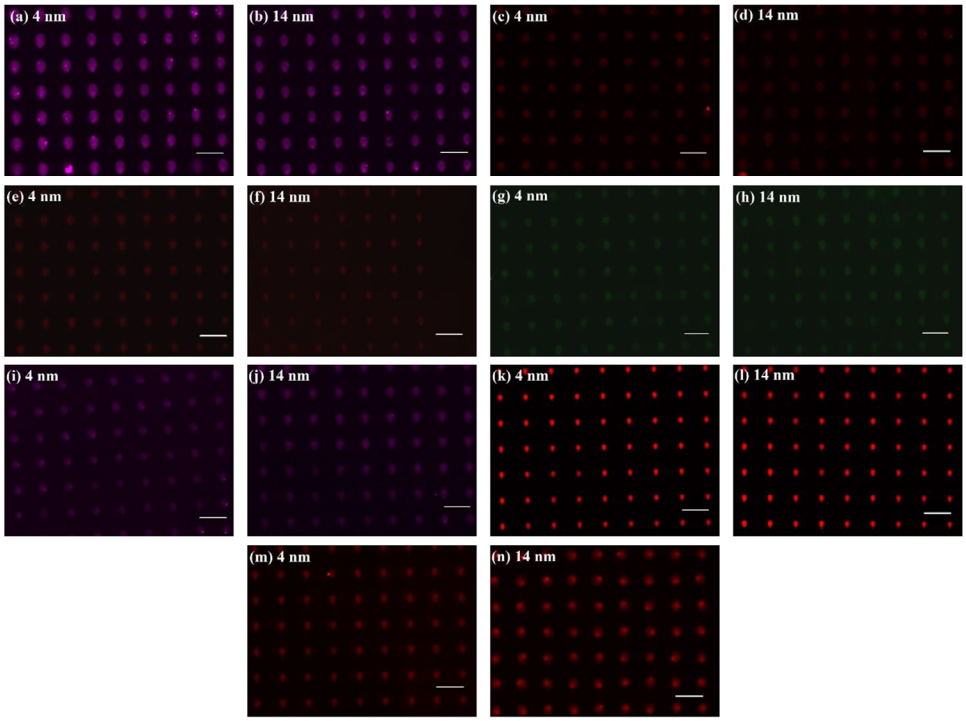

Figure 5. Fluorescence microscopy images of micropatterns of fluorescent inks obtained at optimum reaction conditions with a spotting humidity of 20%, dwell time (tip/surface contact time) of 2 s. Exposure time is 10 s in all images. a,b) Cy5-thiol on a DBCO-terminated surface, c,d) TAMRA-azide on a DBCO-terminated surface, e,f) TAMRA-maleimide on a thiol-terminated surface, g,h) FAM-DBCO on a thiol-terminated surface, i,j) Cy5-thiol on a epoxy-terminated surface, k,l) R6G on an epoxy-terminated surface, and m,n) TAMRA-azide on an epoxy-terminated surface. The scale bars equal 50 µm. Each image shows only a portion of a 15 × 15 spot array and is intended for qualitative visualization.

dibenzocyclooctyne, epoxy, and thiol. These functional groups are often more hydrophobic than the initial surface, particularly in comparison to oxygen-terminated or hydrogenated diamonds.[22] Additionally, surface functionalization can introduce nanoscale roughness, enhancing the hydrophobic effect and increasing the contact angle.[23] Furthermore, the new functional groups may lower the surface energy of the diamond, reducing wettability and leading to an increased contact angle.[24] However, no significant difference in contact angle was observed between the two roughness levels after functionalization.

3.3. Array Immobilization on the Diamond Surfaces

To explore the potential of different click reactions to generate microarrays by µCS, micropatterns of 15 × 15 spots with a pitch of 50 µm were prepared from different fluorescent inks on the different functionalized surfaces. For this purpose, microchannel cantilevers were loaded with a fluorescent ink solution dissolved in dimethyl sulfoxide (DMSO) and supplemented with glycerol to prevent premature drying.[25] Cy5-thiol and TAMRA-azide were used on DBCO-terminated surfaces to perform TYC and SPAAC click reactions, respectively. TAMRA-maleimide and FAM-DBCO were applied to thiol-terminated surfaces for TEMA and TYC click reactions, respectively. Additionally, Cy5-thiol, R6G, and TAMRA-azide were utilized on epoxy-terminated diamonds to facilitate ring-opening click reactions. The reaction conditions were identical to those optimized for glass surfaces, as reported in Table 1. **Figures 5** and **6** present fluorescence microscope images along with the average fluorescence intensity of micropatterns of fluorescent inks obtained under optimal reaction conditions.

The images in Figure 5 show only selected portions of the 15 × 15 spot arrays and are intended for qualitative visualization. Quantitative fluorescence values in Figure 6 were obtained by averaging measurements from 30 spots distributed across multiple regions of each array to account for potential local variations. Brightness differences observed in some image regions arise from minor spotting or drying artifacts and are negligible compared to the overall differences between samples. Similar to glass surfaces, immobilization on diamond appears to have been successful. A significant difference was observed between the two roughness levels, with the fluorescence intensity consistently higher for the 4 nm roughness compared to the 14 nm roughness across all click reactions. This suggests that the click reaction and molecular attachment were more effective on the diamond surface with a roughness of 4 nm. Additionally, surface roughness plays a crucial role in influencing fluorescence intensity. The 4 nm rough surface likely provides a more optimal area for functionalization and subsequent click reactions, enabling a higher density of fluorescent molecule attachment.[14,26] In contrast, the rougher 14 nm surface may contribute to increased fluorescence quenching due to energy transfer between fluorescent molecules and the diamond surface. Smoother surfaces generally exhibit less quenching, leading to higher fluorescence intensity.[27] Moreover, the increased roughness of the 14 nm surface may cause greater light scattering, potentially reducing the

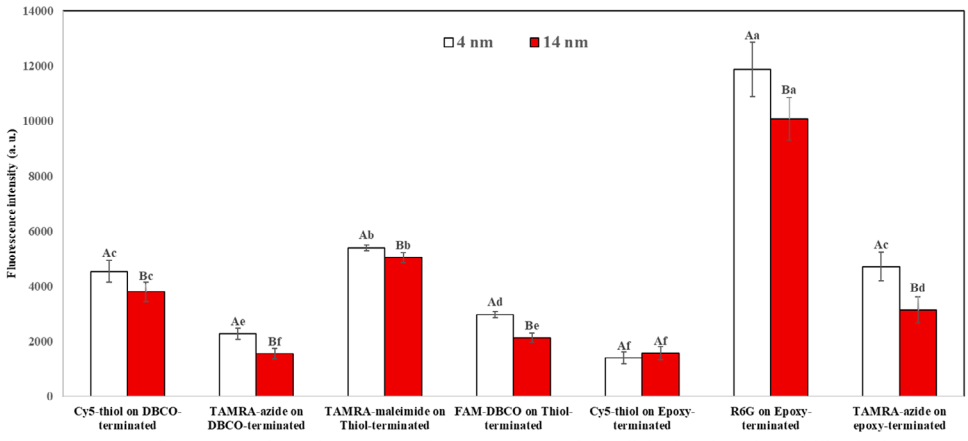

Figure 6. Average fluorescence intensity (measured over 10 spots) of the click-chemistry immobilized microarrays on the differently functionalized diamond surfaces. For the same roughnesses, fluorescence intensity bars with different lower case letters and for the same functional groups, values with different capital letters are significantly different (p <0.05), according to Duncan's test.

detected fluorescence intensity compared to the smoother 4 nm surface.[26,27]

It is important to note that the relative fluorescence intensity varies depending on the type of surface functionalization, so a direct comparison of fluorescence values can only be made between arrays that share the same functionalization but differ in roughness. Variations between different click reactions are expected because each chemistry has a distinct coupling efficiency and surface coverage capability, which can influence signal independently of roughness. For example, while most reactions yielded higher fluorescence on the smoother surface, Cy5-thiol on epoxy-terminated diamond showed no statistically significant difference between 4 nm and 14 nm roughness, likely due to the lower sensitivity of that particular reaction to nanoscale topography. Therefore, Figure 6 is the most relevant dataset for assessing the isolated effect of roughness, as it involves single-step labeling with Cy5 dyes.

3.4. Protein Coupling on the Diamond Surfaces

In the previous section, the successful immobilization of arrays of fluorescent inks on DBCO-, thiol-, and epoxy-terminated diamonds through various click reactions was established. Although the same molar concentration of fluorophores was used for microarray fabrication, a direct comparison between different routes to identify the optimal one is challenging due to the different spectra of the fluorophores, resulting in different emission intensities even at same dye concentration.

Regarding the possibility of separately quantifying the effects of surface roughness versus fluorophore attachment efficiency, in the case of Figures 7 and 8, such a separation is challenging. This is because the two-step modification (biotin functionalization followed by streptavidin binding) involves large biomolecules, and the surface roughness difference (4 nm vs. 14 nm) becomes relatively small compared to the size of the streptavidin molecule (~5–6 nm). At this scale, the contribution of roughness is diminished, and differences in intensity are more likely attributed to the performance of the click chemistry rather than the topography alone. Therefore, an alternative strategy was implemented to enable a direct comparison of the routes.[18a,c] Biotin-bearing compounds were spotted onto the functionalized diamonds using μCS, creating 15 × 15 spot arrays. Biotin is a commonly used linker due to its strong affinity for streptavidin.[28] By utilizing fluorescently-labeled streptavidin as a fluorophore to visualize the immobilized biotin patterns, the amount of immobilized biotin can be compared across different routes.[29]

To confirm that the observed fluorescence resulted from specific biotin–streptavidin binding rather than nonspecific adsorption, we conducted a control experiment in which biotin was immobilized on one diamond surface, while a separate diamond surface was prepared without biotin modification. Streptavidin was then printed across both surfaces, followed by a washing step. After washing, fluorescence was observed only on the biotin-functionalized diamond, while no fluorescence signal was detected on the diamond without biotin. This confirms that streptavidin binding was specific and not due to non-specific adsorption, as shown in **Figure** 9. The results obtained for arrays fabricated under optimal conditions are summarized in **Figures** 7 and 8.

The images in Figure 7 show only selected portions of the 15 × 15 spot arrays and are intended for qualitative visualization. Quantitative fluorescence values in Figure 8 were calculated by averaging measurements from 30 spots distributed across different regions of each array to account for potential local variations. Minor differences in brightness between certain regions of the same image arise from small experimental artifacts during spotting or drying, but these are negligible compared to the overall fluorescence intensity differences between samples. For all chemical routes, the immobilization of the biotinylated compound was successful. After staining the patterns with fluorescently-labeled streptavidin, they were visible in the corresponding fluorescence channel. When comparing the different immobilization routes, it is evident that biotin-amine on the epoxy-terminated diamond (via ring-opening of epoxy by the amine route)[18b] and biotin-maleimide on the thiol-terminated diamond (via thiol-ene Michael addition (TEMA) route)[18c] yield higher fluorescence intensities. These notable findings on

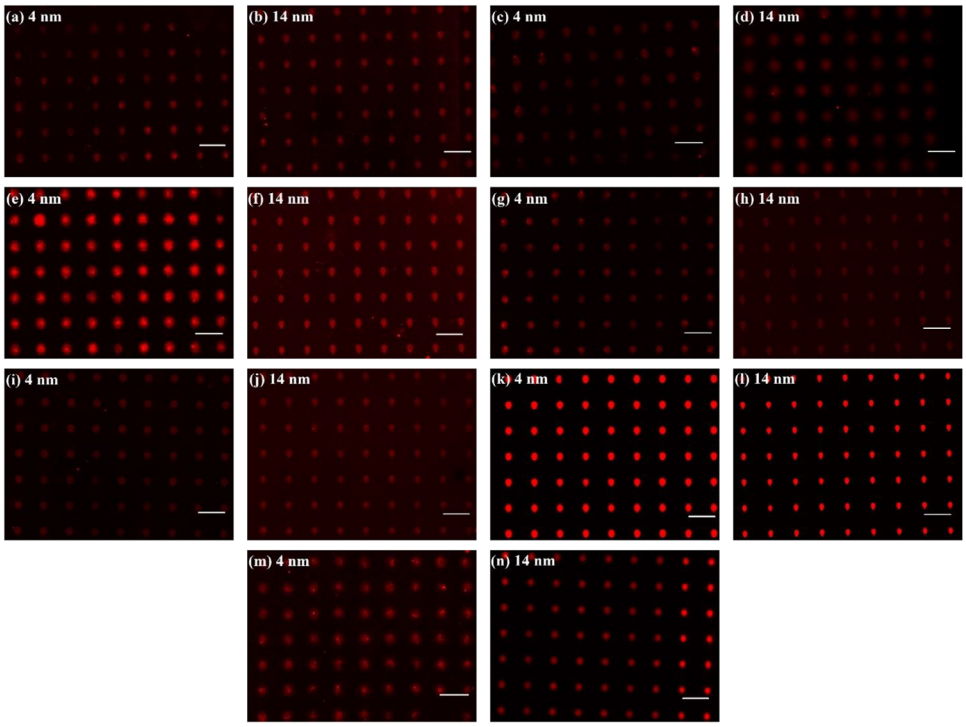

Figure 7. Fluorescence microscopy images of micropatterns of non-fluorescent, biotinylated inks after incubation with fluorescently-labeled streptavidin. The arrays were obtained at optimum reaction conditions with a spotting humidity of 20%, dwell time (tip/surface contact time) of 2 s. Exposure time is 10 s in all images. a,b) biotin-thiol on a DBCO-terminated surface, c,d) biotin-azide on a DBCO-terminated surface, e,f) biotin-maleimide on a thiol-terminated surface, g,h) biotin-DBCO on a thiol-terminated surface, i,j) biotin-thiol on an epoxy-terminated surface, k,l) biotin-amine on an epoxy-terminated surface, and m,n) biotin-azide on an epoxy-terminated surface. The scale bars equal 50 µm. Each image shows only a portion of a 15 × 15 spot array and is intended for qualitative visualization.

diamond surfaces are consistent with previous results obtained for the functionalization of glass surfaces. In earlier studies, we investigated and compared different immobilization approaches, including ring opening, SPAAC, TYC, and TEMA, for the formation of covalently bound microarrays on functionalized glass surfaces. The relative efficiency of these reactions was determined as follows: Ring opening > TEMA > TYC > SPAAC.[18a–d]

The successful binding of streptavidin on the microarrays immobilized on the diamond surfaces indicates that these functionalizations can be used in diamond-based biosensors utilizing biotinylated recognition elements (e.g., antibodies) over a streptavidin-based sandwich approach.[30] More generally, also arbitrary unlabeled proteins can be immobilized on the diamond in this fashion. As proteins are composed of amino acids, which

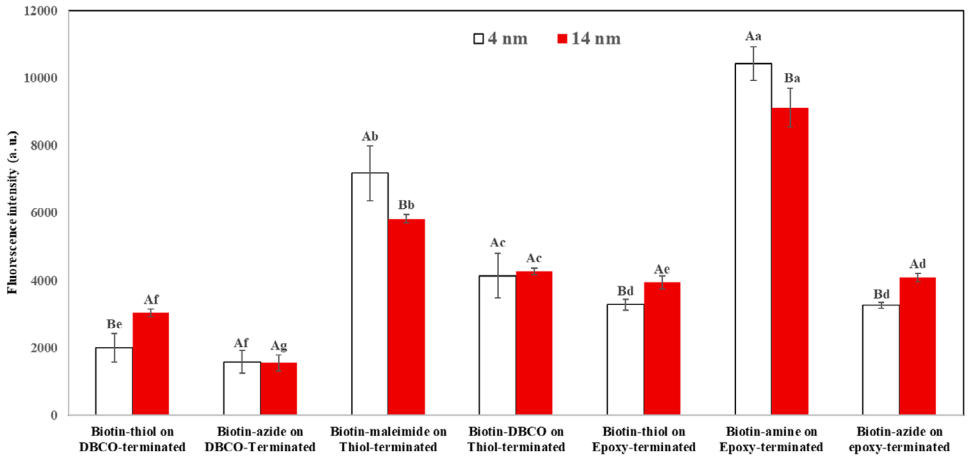

Figure 8. Average fluorescence intensity (measured over 10 spots) of fluorescein-labeled streptavidin on the click-chemistry immobilized biotin-microarrays on the differently functionalized diamond surfaces. For the same roughnesses, fluorescence intensity bars with different lower case letters and for the same functional groups, values with different capital letters are significantly different ($p < 0.05$), according to Duncan's test.

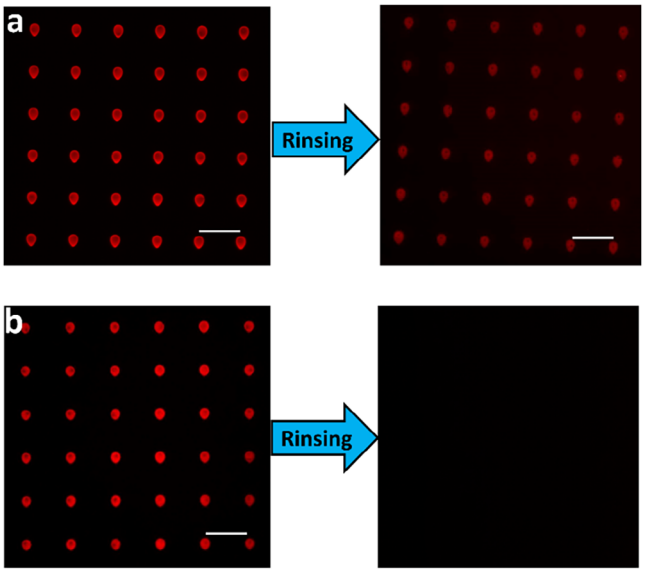

Figure 9. Control experiment confirming specific biotinstreptavidin binding on diamond surfaces. (a) Biotin-functionalized surface retains fluorescence after rinsing. (b) Non-biotin surface shows no fluorescence post-rinsing, indicating minimal nonspecific adsorption. Scale bars: 50 µm.

contain amine groups, these amine groups can react with epoxy through a ring-opening click reaction. Using this technique, arbitrary unlabeled antigens or antibodies can be immobilized on the surface for detection of complementary proteins.

4. Conclusion

We demonstrated novel functionalization routes for diamond-based platforms, integrating optimized surface functionalization via click chemistry for biosensing and controlled surface roughness for enhanced fluorescence. By systematically evaluating multiple click reactions on diamond surfaces, we identified the most efficient immobilization route. Smoother diamond surfaces exhibit significantly higher fluorescence intensity compared to rougher surfaces, which can be attributed to reduced light scattering and functionalization defect density. The optimized surface functionalization and roughness control not only enhance biointerface stability and protein amount of protein adhesion but also improve fluorescence efficiency. These findings establish a strong foundation for future advancements in diamond-based biosensors and photonic devices, particularly in applications requiring highly selective and stable protein detection and high-performance optical properties.

Acknowledgements

This work is partly carried out with the support of the Karlsruhe Nano Micro Facility (KNMF, https://www.knmf.kit.edu), a Helmholtz Research Infrastructure at Karlsruhe Institute of Technology (KIT, https://www.kit.edu). S.M.M.D. and M.H. gratefully acknowledge support by the Deutsche Forschungsgemeinschaft (DFG) under grant HI 1724/3-1. S.M.M.D. acknowledges support by the German Academic Exchange Service (DAAD) and the Karlsruhe House of Young Scientists (KHYS) in the form of a STIBET grant. The authors thank Georgia Lewes-Malandrakis for providing diamond surfaces for the experiments.

Conflict of Interest

The authors declare no conflict of interest.

Declaration of Generative AI and AI-Assisted Technologies in the Writing Process

During the preparation of this work, the authors used OpenAI's tool Chatgpt to enhance the readability, clarity, and fluency of the text. After using this tool, the authors reviewed and edited the content as needed and took full responsibility for the content of the publication.

Data Availability Statement

The data that support the findings of this study are available from the corresponding author upon reasonable request.

Keywords

biosensor, click chemistry, diamond, fluorescence, protein immobilization, surface roughness, surfaces functionalization

Received: April 28, 2025
Revised: August 12, 2025
Published online:

[1] a) C. E. Nebel, B. Rezek, D. Shin, H. Uetsuka, N. Yang, *J. Phys. D: Appl. Phys.* **2007**, *40*, 6443; b) Y. Einaga, J. S. Foord, G. M. Swain, *MRS Bull.* **2014**, *39*, 525; c) N. E. Santos, F. Figueira, M. Neto, F. A. A. Paz, S. S. Braga, J. C. Mendes, *Appl. Sci.* **2022**, *12*, 3000; d) A. Härtl, E. Schmich, J. A. Garrido, J. Hernando, S. C. Catharino, S. Walter, P. Feulner, A. Kromka, D. Steinmüller, M. Stutzmann, *Nat. Mater.* **2004**, *3*, 736.

[2] a) Q. Zhang, M. Zhang, Y. Du, B. Xu, G. Chen, S. He, D. Zhang, Q. Li, H.-X. Wang, *Diamond Relat. Mater.* **2023**, *134*, 109775; b) C. J. Wort, R. S. Balmer, *Mater. Today* **2008**, *11*, 22; c) Y. Xue, X. Feng, S. C. Roberts, X. Chen, *Funct. Diam.* **2022**, *1*, 221; d) S. Szunerits, C. E. Nebel, R. J. Hamers, *MRS Bull.* **2014**, *39*, 517; e) S. Szunerits, R. Boukherroub, *J. Solid State Electrochem.* **2008**, *12*, 1205; f) C. E. Nebel, N. Yang, S. Yamasaki, *Carbon* **2021**, *182*, 711; g) X. Zhao, W. Hu, *Surf. Interfaces* **2024**, *46*, 104178.

[3] S. K. Kang, S. W. Hwang, H. Cheng, S. Yu, B. H. Kim, J. H. Kim, Y. Huang, J. A. Rogers, *Adv. Funct. Mater.* **2014**, *24*, 4427.

[4] a) Y. Inoue, Y. Yoshimura, Y. Ikeda, A. Kohno, *Colloids Surf., B* **2000**, *19*, 257; b) T. Tsubota, S. Tanii, S. Ida, M. Nagata, Y. Matsumoto, *Phys. Chem. Chem. Phys.* **2003**, *5*, 1474; c) R. J. Nemanich, J. A. Carlisle, A. Hirata, K. Haenen, *MRS Bull.* **2014**, *39*, 490; d) S. Sasi, G. Marappan, Y. Sivalingam, M. Chandran, G. Magna, S. V. Jayaraman, R. Paolesse, C. Di Natale, *Surf. Interfaces* **2024**, *50*, 104456.

[5] M. Kosovari, T. Buffeteau, L. Thomas, A. e.-A. Guay Bégin, L. Vellutini, J. D. McGettrick, G. Laroche, M.-C. Durrieu, *ACS Appl. Mater. Interfaces* **2024**.

[6] G. Primc, M. Mozetič, *Materials* **2024**, *17*, 1494.

[7] S. Wang, Z. Wang, J. Li, L. Li, W. Hu, *Mater. Chem. Front.* **2020**, *4*, 692.

[8] C. Ding, X. Qin, Y. Tian, B. Cheng, *J. Membr. Sci.* **2022**, *659*, 120789.

[9] S. A. Mahadik, S. S. Mahadik, *Ceram. Int.* **2021**, *47*, 29475.

[10] J. Xia, P. Zhao, K. Zheng, C. Lu, S. Yin, H. Xu, *Angew. Chem.* **2019**, *131*, 552.

[11] a) H. C. Kolb, M. Finn, K. B. Sharpless, *Angew. Chem., Int. Ed.* **2001**, *40*, 2004; b) J. Gopinathan, I. Noh, *Tissue Eng. Regener. Med.* **2018**,

15, 531; c) J. Hou, X. Liu, J. Shen, G. Zhao, P. G. Wang, *Expert Opin. Drug Discov.* **2012**, *7*, 489; d) M.-M. Chen, P. M. Kopittke, F.-J. Zhao, P. Wang, *Trends Plant Sci.* **2024**; e) L. Xu, J. Dong, *Chin. J. Chem.* **2020**, *38*, 414; f) J. Kaur, M. Saxena, N. Rishi, *Bioconjugate Chem.* **2021**, *32*, 1455.

[12] N. Siegel, H. Hasebe, G. Chiarelli, D. Garoli, H. Sugimoto, M. Fujii, G. P. Acuna, K. Kołątaj, *J. Am. Chem. Soc.* **2024**.

[13] D. Wang, Y. Gao, S. Gao, H. Huang, F. Min, Y. Li, S. Seeger, J. Jin, Z. Chu, *J. Membr. Sci.* **2023**, *670*, 121336.

[14] R. Kumar, B. Yang, J. Barton, M. Stejfova, A. Schäfer, M. Koenig, P. Knittel, P. Cigler, M. Hirtz, *Adv. Mater. Interfaces* **2022**, *9*, 2201453.

[15] M. Xie, X. Yu, L. V. Rodgers, D. Xu, I. Chi-Durán, A. Toros, N. Quack, N. P. de Leon, P. C. Maurer, *Proc. Natl. Acad. Sci. U.S.A.* **2022**, *119*, 2114186119.

[16] H. Martin-Gómez, L. Oliver-Cervelló, I. Sanchez-Campillo, V. Marchán, M.-P. Ginebra, C. Mas-Moruno, *Chem. Commun.* **2021**, *57*, 982.

[17] Y. Zhang, J. Shen, R. Hu, X. Shi, X. Hu, B. He, A. Qin, B. Z. Tang, *Chem. Sci.* **2020**, *11*, 3931.

[18] a) S. M. M. Dadfar, S. Sekula-Neuner, U. Bog, V. Trouillet, M. Hirtz, *Small* **2018**, *14*, 1800131; b) S. M. M. Dadfar, S. Sekula-Neuner, V. Trouillet, M. Hirtz, *Adv. Mater. Interfaces* **2021**, *8*, 2002117; c) S. M. M. Dadfar, S. Sekula-Neuner, V. Trouillet, M. Hirtz, *Adv. Mater. Interfaces* **2018**, *5*, 1801343; d) S. M. M. Dadfar, S. Sekula-Neuner, V. Trouillet, H.-Y. Liu, R. Kumar, A. K. Powell, M. Hirtz, *Beilstein J. Nanotechnol.* **2019**, *10*, 2505; e) B. Yang, K. Gordiyenko, A. Schäfer, S. M. M. Dadfar, W. Yang, K. Riehemann, R. Kumar, C. M. Niemeyer, M. Hirtz, *Adv. NanoBiomed Res.* **2023**, *3*, 2200133.

[19] a) O. A. Williams, O. Douhéret, M. Daenen, K. Haenen, E. Ōsawa, M. Takahashi, *Chem. Phys. Lett.* **2007**, *445*, 255; b) M. Füner, C. Wild, P. Koidl, *Appl. Phys. Lett.* **1998**, *72*, 1149.

[20] A. De Oliveira, F. Placias, A. da Silva Sobrinho, D. Leite, W. Miyakawa, J. J. Neto, I. Koh, A. Liberatore, M. dos Santos, J. Matieli, *Thin Solid Films* **2021**, *719*, 138487.

[21] a) S. Krainer, U. Hirn, *Colloids Surf. A* **2021**, *619*, 126503; b) G. McHale, R. Ledesma-Aguilar, C. Neto, *Langmuir* **2023**, *39*, 11028.

[22] a) N. M. Sulthana, K. Ganesan, P. Ajikumar, S. Dhara, *Diamond Relat. Mater.* **2022**, *128*, 109284; b) Y. Tian, A. R. Ortiz Moreno, M. Chipaux, K. Wu, F. P. Perona Martinez, H. Shirzad, T. Hamoh, A. Mzyk, P. van Rijn, R. Schirhagl, *Langmuir* **2024**, *40*, 23007.

[23] M. Mertens, M. Mohr, K. Bruehne, H.-J. Fecht, M. Łojkowski, W. Święszkowski, W. Łojkowski, *Appl. Surf. Sci.* **2016**, *390*, 526.

[24] a) M. S. Sammon, S. Schirra, M. F. Pill, H. Clausen-Schaumann, M. K. Beyer, *Chem.-Methods* **2021**, *1*, 271; b) W. Alnoush, A. Sayed, T. I. Solling, N. Alyafei, *J. Pet. Sci. Eng.* **2021**, *203*, 108679.

[25] M. Hirtz, A. M. Greiner, T. Landmann, M. Bastmeyer, H. Fuchs, *Adv. Mater. Interfaces* **2014**, *1*, 1300129.

[26] P. Chrostoski, P. Kehayias, D. Santamore, *Phys. Rev. B* **2022**, *106*, 235311.

[27] J. J. Sakon, G. J. Ribeill, J. M. Garguilo, J. Perkins, K. R. Weninger, R. J. Nemanich, *Diamond Relat. Mater.* **2009**, *18*, 82.

[28] a) C. M. Dundas, D. Demonte, S. Park, *Appl. Microbiol. Biotechnol.* **2013**, *97*, 9343; b) S. Jung, H. Yi, *Biomacromolecules* **2013**, *14*, 3892.

[29] H. Seto, C. Yamashita, S. Kamba, T. Kondo, M. Hasegawa, M. Matsuno, Y. Ogawa, Y. Hoshino, Y. Miura, *Langmuir* **2013**, *29*, 9457.

[30] U. Bog, F. Brinkmann, H. Kalt, C. Koos, T. Mappes, M. Hirtz, H. Fuchs, S. Köber, *Small* **2014**, *10*, 3863.